

Chromospheres in Metal-Poor Stars Evidenced from the He I 10830 Å Line *

Yoichi TAKEDA

National Astronomical Observatory of Japan 2-21-1 Osawa, Mitaka, Tokyo 181-8588
takeda.yoichi@nao.ac.jp

and

Masahide TAKADA-HIDAI

Liberal Arts Education Center, Tokai University, 4-1-1 Kitakaname, Hiratsuka, Kanagawa 259-1292
hidai@apus.rh.u-tokai.ac.jp

(Received 2010 November 5; accepted 2010 December 24)

Abstract

Based on the near-IR spectra of 33 late-type stars in the wide metallicity range (mainly dwarfs and partly giants) obtained with IRCS+AO188 of the Subaru Telescope, we confirmed that He I 10830 Å line is seen in absorption in almost all moderately to extremely metal-poor stars of thick disk and halo population (from $[\text{Fe}/\text{H}] \sim -0.5$ down to $[\text{Fe}/\text{H}] \sim -3.7$), the strength of which is almost constant irrespective of the metallicity. This is an evidence that chromospheric activity at a basal level persists even for such old stars, despite that their rotations are considered to be slowed down and incapable of sustaining a dynamo, suggesting that some kind of chromospheric heating mechanism independent of rotation/magnetism (e.g., acoustic heating) may take place.

Key words: stars: activity — stars: chromospheres — stars: late-type
 — stars: population II

1. Introduction

It is not well understood whether and how the chromosphere (temperature rise phenomenon in the upper atmosphere), which is confirmed in the Sun and nearby solar-type stars, exists in old metal-poor stars.

A useful guideline for considering this problem is the positive correlation between the chromospheric emission and surface rotation among cool (young to solar age) stars (Noyes et al. 1984), which can be rephrased as the activity–age relation (Skumanich law), since rotation is generally decelerated with age as a result of magnetic braking (i.e., loss of angular momentum caused by stellar wind pulling out magnetic field lines). This observational fact is generally interpreted by the scenario that globally-organized magnetic field generated by differential rotation-induced dynamo is essentially responsible for the origin of the chromospheric activity. Then, we may expect that any chromospheric activity would have almost come to rest in such aged stars, as they are likely to be rotating very slowly (i.e., practically non-rotating) due to the long-lasting gradual deceleration they have suffered.

Meanwhile, contrary to this naive expectation, there are indications that chromospheres *do* exist even in very old population II stars. For example, Dupree, Smith, and Strader (2009) recently showed, in their extensive studies on the infrared He I line at 10830 Å (hereinafter often abbreviated as “He I 10830”) for 41 metal-deficient G–

K giants, that this high-excitation line arising from the metastable level ($2s^3S_1$, $\chi_{\text{low}} = 19.72$ eV) is ubiquitously observed with appreciable blue shift for stars with $T_{\text{eff}} \gtrsim 4500$ K, indicating the existence of outward-moving high-temperature chromospheric layer. Actually, detections of chromospheric emission in the core of Mg II $h+k$ doublet at 2800 Å were also reported for 10 population II giants by Dupree, Hartmann, and Smith (1990).

Yet, it is not clear from this fact alone whether the chromospheric heating mechanism similar to the solar case is operative in these evolved red giants, since some other physical process specific to the unstable low-density atmosphere may be responsible for this activity (for example, pulsation-induced shock dissipation; e.g., Smith & Dupree 1988). Therefore, in order to see how the solar-type chromospheres go through changes towards metal-poor regime, one should study the activity of unevolved population II “dwarfs.”

As to activities of metal-poor dwarfs, we know only a few researches. Smith and Churchill (1998) investigated the cores of Ca II H+K lines in 23 metal-poor dwarfs, and found signs of chromospheric emission in some halo stars with metallicities as low as $[\text{Fe}/\text{H}] \sim -2$, while negative results were also obtained for not a few cases. Peterson and Schrijver (1997) detected chromospheric emissions of Mg II $h+k$ 2800 lines (being superior to Ca II H+K lines for detecting chromospheric core emissions, because of the difference in the line- as well as continuum-opacities) in all (~ 10) metal-poor solar-type stars down to $[\text{Fe}/\text{H}] \sim -2.60$ they searched, which indicates that chromospheres ubiquitously exist in population II halo dwarfs. Peterson

* Based on data collected at Subaru Telescope, which is operated by the National Astronomical Observatory of Japan.

and Schrijver (2001) further confirmed the existence of Lyman α emission in their sample of halo stars (though the contamination of interstellar absorption and geocoronal emission made any detailed line-profile study rather difficult), which substantiates their conclusion.

Though these studies invoking the emission in the core of strong metal-lines (Ca II H+K or Mg II $h+k$) are regarded as important, since the existence of chromospheres in old population II dwarfs has been revealed in the qualitative sense, they are not necessarily informative when it comes to quantitatively studying whether or not the degree of activity varies with the metallicity, since the extent of core emission in such metallic lines would depend on the metallicity even if the extent of activity remains unchanged; also, its usability is not clear for extremely metal-poor regime (e.g., $[\text{Fe}/\text{H}] \lesssim -3$).

From this viewpoint, the most desirable way to investigate the chromospheric activity of metal-poor solar-type stars is to use the He I 10830 line, since it is a chromospheric indicator practically independent of the metallicity. Admittedly, several extensive studies on the He I 10830 line for solar-type stars have been published so far (e.g., Vaughan & Zirin 1968; Zirin 1982; Zarro & Zirin 1986; O’Brien & Lambert 1986; Lambert 1987; see also the references cited in Andretta & Giampapa 1995). Somewhat unexpectedly, however, any observation of the He I 10830 line seems to have never been reported for “metal-poor dwarfs of population II” to our knowledge.

Timely, we have recently obtained near-IR (zJ -band) spectra of 33 disk/halo stars (mainly dwarfs and partly giants) covering a wide metallicity range ($-3.7 \lesssim [\text{Fe}/\text{H}] \lesssim +0.3$), and carried out sulfur abundance determinations based on the S I triplet lines at 10455–10459 Å (Takeda & Takada-Hidai 2011; hereinafter referred to as Paper I). Therefore, we decided to examine the He I 10830 line in the spectra of these stars with an aim to see how the chromospheric activity behaves itself in metal-poor stars, while checking if this line is visible and how its strength varies from star to star with a change of metallicity. This is the purpose of this investigation.

2. Observational Data

The list of the program stars, 33 halo/disk stars (24 dwarfs and 9 giants¹) in the metallicity range of $-3.7 \lesssim [\text{Fe}/\text{H}] \lesssim +0.3$, is presented in table 1, where the literature values of the atmospheric parameters (the same as in Paper I), apparent V magnitudes (from SIMBAD database), and $\log(f_{\text{x}}/f_{\text{bol}})$ values (ratio of the X-ray flux to the total bolometric flux) available in ROSAT archival data (accessible from the HEASARC web site²) are also

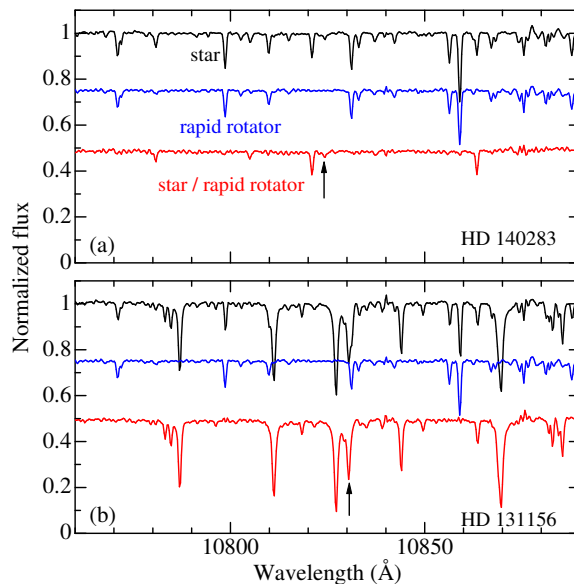


Fig. 1. Examples demonstrating how the telluric lines (mostly due to H₂O vapor) could be removed in the spectra used for measuring the He I 10830 line. Dividing the raw stellar spectrum (top, black) by the spectrum of a rapid rotator γ Tri (middle, with an offset of -0.25 ; blue) results in the final spectrum (bottom, with an offset of -0.5 ; red). The upper panel (a) and lower panel (b) show the typical metal-poor case (HD 140283) and the metal-rich case (HD 131156), respectively. No Doppler correction is applied to the wavelength scale of these spectra. The arrow indicates the position of the He I 10830 line.

given. The observational data are the zJ -band (1.04–1.19 μm) spectra with $R \sim 20000$ (wavelength resolution) and $S/N \sim 100$ –200 (signal-to-noise ratio; ~ 300 only for BD+44°493), which were obtained on 2009 July 29 and 30 (UT) with the Infrared Camera and Spectrograph (IRCS) along with the 188-element curvature-based adaptive optics system (AO188) of the Subaru Telescope. See section 2 of Paper I for the details of the observation and the data reduction procedure.

Since several appreciable telluric lines (due to H₂O vapor) are located in the neighborhood of the He I 10830 line, we removed them by dividing each stellar spectrum by that of a rapid rotator (γ Tri) with the help of the task “telluric” in IRAF.³ This procedure turned out quite successful, as shown in figure 1. The finally resulting spectra, which were used for measuring the He I 10830 line, are displayed in figure 2. Regarding the Sun, we adopted the solar flux spectrum published by Kurucz et al. (1984).

3. Measurement of the He I 10830 Feature

The He I 10830 Å triplet ($2s^3S_1 - 2p^3P_{0,1,2}$) comprises three components at 10829.088, 10830.247, and

¹ As in Paper I, the targets are divided according to the surface gravity into two classes (those with $\log g < 3$ and $\log g > 3$), which we tentatively call “giants” and “dwarfs,” respectively. It should thus be kept in mind that “dwarfs” includes some stars actually classified as subgiants. Besides, in this paper, giants with $\log g < 2$ are particularly called as “low-gravity giants” (cf. table 1), since they tend to show anomalous He I 10830 line profiles.

² (<http://heasarc.gsfc.nasa.gov/>).

³ IRAF is distributed by the National Optical Astronomy Observatories, which is operated by the Association of Universities for Research in Astronomy, Inc. under cooperative agreement with the National Science Foundation.

10830.336 Å (with $\log gf$ of -0.745 , -0.268 , and -0.047 , respectively).⁴ However, since the first component is considerably weaker than and separated from the others, the latter two close components essentially determine the position of the stellar He I 10830 line.

First of all, the important fact manifestly recognized from figure 2 is that this He I line is clearly visible (in absorption) in most of the program stars; i.e., not only metal-rich stars of disk population but also old very metal-poor stars (even in the extremely metal-poor star BD+44°493 with $[\text{Fe}/\text{H}] \simeq -3.7$). This is a reconfirmation of the previous report (based on Ca II, Mg II, and Ly α lines) that chromospheres ubiquitously exist in old population II solar-type stars (Smith & Churchill 1998; Peterson & Schrijver 1997, 2001); but our result substantiates this fact in a more convincing manner for a larger number of stars in a much wider metallicity range than ever before.

The equivalent width (EW) of the He I 10830 line was evaluated for each star by the Gaussian fitting, as depicted in figure 2. We tried to measure EW as long as (i) the center of the absorption feature situates at almost the expected wavelength of the He I 10830 line, and (ii) the line profile is not too severely blended.

Generally, “low-gravity” giants (with $\log g < 2$) tend to show appreciably blue-shifted components, making the profile complex or blended with the neighboring Si I line at 10827.1 Å, which must be due to the significant gas outflow typically seen in red-giant atmospheres (e.g., Dupree et al. 2009). So we had to abandon measuring EW s for four low-gravity giants (HD 122563, HD 204543, HD 121135, and Arcturus). As a result, since the EW data for “giants” (with $\log g < 3$) turned out insufficient (only five stars), we will focus our discussion only on the 24 “dwarf” stars in the remainder of this paper (unless otherwise specially noted), given that the main aim of this paper is to investigate the chromospheric activity of population II “solar-type” stars.

The line-depth (R_0), the full-width at half-maximum ($fwhm$), and the equivalent width (EW) corresponding to the fitted Gaussian profile are given in table 1, while figure 3 shows how the resulting $\log EW$ values are correlated with $[\text{Fe}/\text{H}]$.

Uncertainties in EW caused by photometric random errors may be estimated by invoking the formula derived by Cayrel (1988), who showed that the ambiguity in EW is roughly expressed as $\sim 1.6(w \delta x)^{1/2} \epsilon$, where w is the typical line FWHM, δx is the pixel size (in unit of wavelength), and ϵ is the photometric accuracy represented by $\sim (\text{S/N})^{-1}$. Substituting $w \sim 1$ Å, $\delta x \simeq 0.25$ Å, and $\epsilon \sim 1/100$, we obtain ~ 8 mÅ as the uncertainty in EW . Considering that typical EW is ~ 30 mÅ in the present case, corresponding to $\sim \pm 0.1$ dex in $\log EW$. Meanwhile, since the continuum level could be reasonably defined to $\lesssim 10$ –20% of the line-depth for most of the cases (cf. figure 2), the errors in $\log EW$ due to uncertainties in the con-

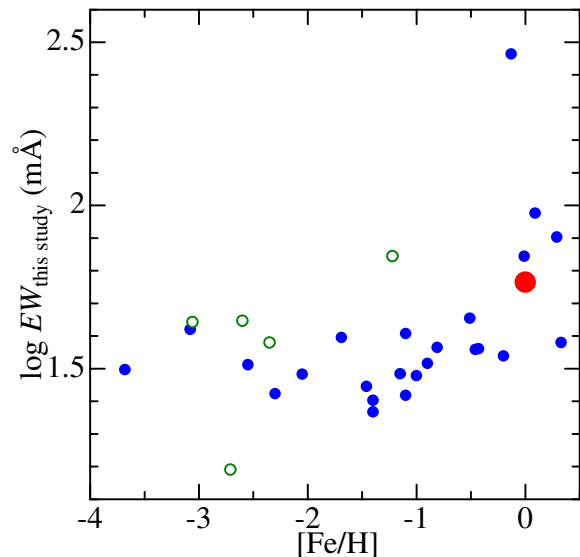


Fig. 3. Logarithmic equivalent width ($\log EW$) measured for the He I 10830 line, plotted against the metallicity ($[\text{Fe}/\text{H}]$). The results for 24 dwarfs ($\log g > 3$) and 9 giants ($\log g < 3$) are discriminated by filled (blue) and open (green) symbols, respectively. The Sun is indicated by the large (red) filled circle.

tinuum placement are estimated to be again $\lesssim 0.1$ dex. Accordingly, combining these two factors, we may state that the ambiguity in $\log EW$ is on the order of $\sim \pm 0.1$ dex (~ 20 –30% in EW).

4. Discussion

4.1. Characteristics in the Behaviors of $EW(\text{He I } 10830)$

An inspection of figure 3 reveals the following notable characteristics. While we can not say much about giants (open circles) because of their paucity, which tend to show a rather large spread between $\log EW(\text{mÅ}) \sim 1$ and ~ 2 , dwarfs (filled circles) exhibit a significant trend in terms of the metallicity. That is, its strength is nearly constant around $\log EW(\text{mÅ}) \sim 1.5$ over the wide metallicity range of $-3.7 \lesssim [\text{Fe}/\text{H}] \lesssim -0.5$, while it tends to somewhat strengthen (in the average sense) up to $\log EW(\text{mÅ}) \sim 2$ for comparatively metal-rich stars at $-0.5 \lesssim [\text{Fe}/\text{H}]$ (HD 131156 = ξ Boo A shows an exceptionally large strength of $\log EW(\text{mÅ}) \sim 2.5$, which is a well-known active star with large spots on its surface as characterized by the detection of its magnetic field by Robinson et al. 1980).

For the purpose of corroborating this relation, we increased the data points by adding the literature results taken from Zarro and Zirin (1986) and Dupree et al. (2009) as displayed separately for dwarfs (figure 4a) and giants (figure 4b). Considering the large variation of $EW(\text{dwarfs})$ in the metal-rich domain around $[\text{Fe}/\text{H}] \sim 0$ as manifestly seen in figure 4a, we may regard that such an apparent increase in the (averaged) $EW(\text{dwarfs})$ at $-0.5 \lesssim [\text{Fe}/\text{H}]$ seen in our data (figure 3) simply re-

⁴ Data from the Vienna Atomic Line Database (<http://vald.astro.univie.ac.at/>).

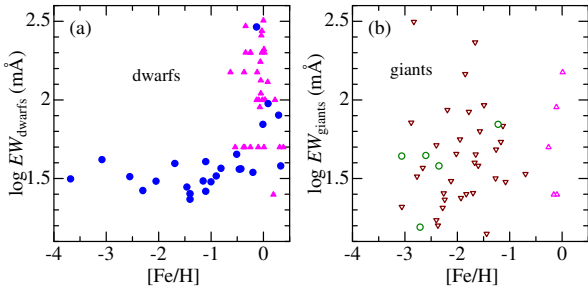


Fig. 4. Comparison of the $\log EW(10830)$ vs. $[\text{Fe}/\text{H}]$ relation derived from this study with that from the literature data. Panels (a) and (b) correspond to dwarfs (filled symbols) and giants (open symbols), respectively. Circles ... this study (same colors as in figure 3); triangles (pink) ... Zarro and Zirin’s (1986) compilation (EW) along with Cayrel de Strobel’s (2001) catalogue ($[\text{Fe}/\text{H}]$); inverse triangles (brown) ... Dupree et al. (2009).

reflects the difference in the dispersion of $EW(\text{dwarfs})$ between the $[\text{Fe}/\text{H}] \lesssim -0.5$ group (small dispersion) and $-0.5 \lesssim [\text{Fe}/\text{H}]$ group (considerably large dispersion). It may be worth stressing that such a near-constancy in EW for metal-poor stars at $[\text{Fe}/\text{H}] \lesssim -0.5$ is restricted to “dwarf” stars, since $EW(\text{giants})$ show a considerably large scatter irrespective of the metallicity (figure 4b).

Further, we plotted the measured EW against $\log(f_x/f_{\text{bol}})$ observed by ROSAT (available only 8 apparently bright dwarf stars of $V \lesssim 5$ at $-0.9 \lesssim [\text{Fe}/\text{H}]$; cf. table 1) in figure 5. We can see from this figure that our data reasonably follow the tendency exhibited by the various published data compiled by Zarro and Zirin (1986).

4.2. Origin of Chromospheres

From the viewpoint of the kinematic properties, the two metallicity groups (roughly divided at $[\text{Fe}/\text{H}] -0.5$) mentioned in the previous subsection are markedly different from each other (see figure 1 in Paper I); i.e., the former is “halo or thick-disk stars” (older than the Sun) while the latter is “thin-disk stars” (near-solar age or younger stars). Considering the importance of rotation in the conventional understanding of stellar activity described in section 1, we may speculate that different types of chromospheres are involved between these two cases:

- (1) For comparatively young thin-disk stars ($-0.5 \lesssim [\text{Fe}/\text{H}]$; where a markedly large dispersion in EW is observed), which still show appreciable rotational velocities, stellar rotation plays the decisive role in controlling the chromospheric activity, for which organized magnetic fields generated by a dynamo (which is induced by the differential rotation) are responsible.
- (2) For older halo or thick-disk stars ($-3.7 \lesssim [\text{Fe}/\text{H}] \lesssim -0.5$; where EW is almost constant) whose rotations are supposed to have been considerably slowed down, the standard rotation/magnetism-induced heating mechanism does not work efficiently any more. Instead, a chromospheric activity at the “basal” or minimum level

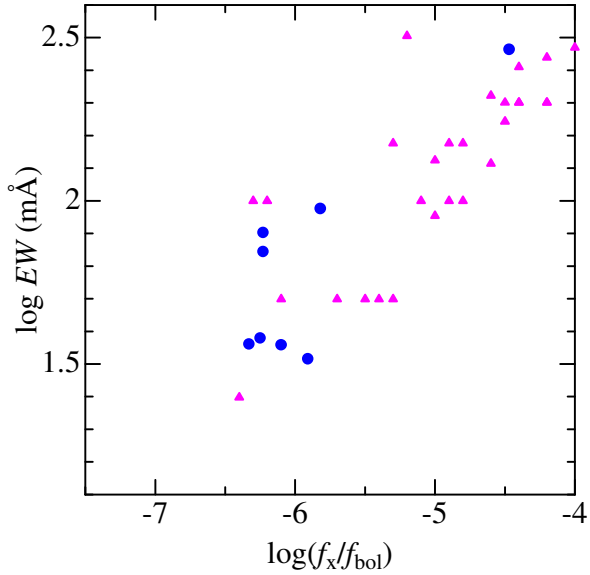


Fig. 5. Logarithmic He I 10830 line strength ($\log EW$) plotted against X-to-bolometric flux ratio ($\log(f_x/f_{\text{bol}})$). Circles (blue) ... EW data derived in this study compared with the ROSAT data (cf. table 1); triangles (pink) ... published data compiled by Zarro and Zirin (1986). Note that all the data shown here are for dwarf stars, since available X-ray data are essentially limited to apparently bright dwarfs.

(e.g., Schrijver 1987; Rutten et al. 1991) comes into sight, which is maintained irrespective of stellar rotation. Regarding the specific mechanism responsible for such a “basal” chromosphere, acoustic waves generated by convection (apparently independent of rotation) may be promising (e.g., Schrijver 1995; Narain & Ulmschneider 1996; see also the discussion in Peterson & Schrijver 1997, 2001).

We point out that, in order to test the “basal chromosphere” scenario mentioned above, long-term observations (over ~ 10 years or more) monitoring the activity of old metal-poor stars may be worth carrying out, since those stars would not show any near-cyclic activity variation such as that exhibited by the Sun or nearby solar-type stars. The He I 10830 line (a good chromospheric indicator as evidenced by its close connection with the Ca II H+K core emission in the Sun seen as a star; e.g., Livingston et al. 2007) would be most suitable for this purpose, as it can be used even for extremely metal-deficient stars (unlike Ca II H+K) and its observation can be done from the ground (unlike Mg II $h+k$ or Lyman α).

4.3. Rotations of Metal-Poor Stars

To make this discussion complete, we should remark that our argument is based on the (intuitively reasonable) postulation that rotational velocities of old metal-poor stars are appreciably slowed down compared with those of younger metal-rich stars. It is thus important to check if such a tendency is really observed. But embarrassingly, according to the literature data compiled by Cortés et al.

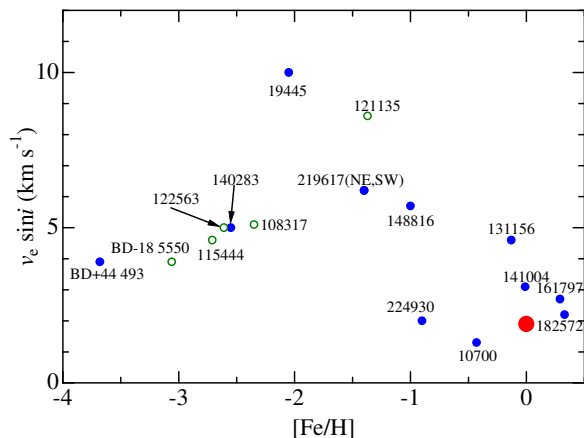


Fig. 6. Published values of the projected rotational velocity ($v_e \sin i$) plotted against the metallicity ($[\text{Fe}/\text{H}]$) for 17 stars (among the 33 targets in this study) for which literature data are available. We consulted Cortés et al.’s (2009) compilation for 11 metal-poor stars with $[\text{Fe}/\text{H}] \leq -1$, the Bright Star Catalog (Hoffleit & Jaschek 1982) only for HD 224930 ($[\text{Fe}/\text{H}] = -0.9$), and Valenti and Fischer (2005) for 5 stars with $-0.5 < [\text{Fe}/\text{H}]$. The corresponding star designations are indicated in the figure. The meanings of the symbols are the same as in figure 3.

(2009), metal-deficient stars ($[\text{Fe}/\text{H}] \lesssim -1$) in our sample show even *higher* $v_e \sin i$ values than metal-rich stars as shown in figure 6, which is just the opposite to our expectation. However, considering the enormous difficulty involved with $v_e \sin i$ determinations of slow rotators as low as $\lesssim 1\text{--}2 \text{ km s}^{-1}$ (i.e., contribution of the macroturbulence is almost predominant over the rotational effect on the line profile), we are still conservative and rather reluctant to take these results seriously, which are based on not-so-high quality spectra and subject to errors on the same order of the $v_e \sin i$ values themselves (cf. table 1 of Cortés et al. 2009).⁵ In any event, if it were really confirmed based on reliable observations that rotations of old stars are not decelerated (or even accelerated), then we would have to earnestly reconsider the stellar activity of metal-poor stars in a completely different paradigm.

4.4. Impact of Chromospheres upon Spectral Line Formation

Given that the existence of high-temperature layer ($T \sim 10^4 \text{ K}$) in the upper atmosphere of any solar-type stars (regardless of the metallicity) has been established, we have some concern about whether this effect may have any influence on the analysis of stellar spectra (e.g., chemical

abundance determinations), where conventional model atmospheres (with monotonically decreasing temperatures outwards) are exclusively relied upon. Actually, the same situation applied even in the recent state-of-the-art 3D inhomogeneous hydrodynamical model atmospheres, where the averaged temperatures are nearly the same (for the solar metallicity) or even appreciably *lowered* (for the metal-poor condition) compared to the classical 1D model (see, e.g., figures 1 and 2 in Asplund 2005), reflecting the fact that any physical process (e.g., dissipation of acoustic energy) leading to formation of chromospheres is not included in the current 3D models. Thus, such a difference in the temperature structure may have some appreciable effect on the spectral line formation (especially for high-forming strong lines), though it is not easy to make a general prediction without any detailed calculation. For example, the core flux of the strong Ca II lines (e.g., doublet lines at 3934/3968 Å or triplet lines at 8498/8542/8662 Å) tends to be raised by an increase in the surface temperature (cf. Appendix B in Takeda et al. 2010). On the contrary, the core of the high-excitation O I lines (e.g., triplet lines at 7771–5 Å or 8446 Å) gets *deepened* (though slightly) by the chromospheric temperature rise, as shown by Takeda (1995).

Besides, even for ordinary (comparatively weak) spectral lines, which are deep-forming and appear to be practically unaffected by any temperature structure in high optically-thin layers, a *non-local* effect of chromospheric radiation could be of significance, since emission of photons followed by electron recombination is considerably enhanced in the chromosphere reflecting that recombination rates are sensitive to the local electron temperature (T_e) with a dependence of $\propto \exp(-h\nu/kT_e)$ (where Wien’s approximation is hold; h : Planck constant, k : Boltzmann constant). This effect might influence the ionization equilibrium of any element, especially in metal-deficient atmospheres where such extra radiation of chromospheric origin has a higher possibility to reach the lower photosphere without being absorbed.

5. Conclusion

Based on the near-IR spectra of 33 late-type stars (9 giants and 24 dwarfs) in the wide metallicity range ($-3.7 \lesssim [\text{Fe}/\text{H}] \lesssim +0.3$), which were obtained with IRCS+AO188 of the Subaru Telescope, we examined whether the He I 10830 line is visible and how its strength behaves itself in the metal-poor regime, in order to investigate the chromospheric activity in these stars.

We confirmed that this line is seen in absorption in almost all stars; i.e., not only metal-rich stars of disk population but also extremely metal-poor stars (down to $[\text{Fe}/\text{H}] \simeq -3.7$). This manifestly indicates that chromospheres ubiquitously exist in these FGK-type stars regardless of the metallicity or age.

The equivalent width of this line turned out nearly constant at $\log EW(\text{m}\text{\AA}) \sim 1.5$ over the wide metallicity range of $-3.7 \lesssim [\text{Fe}/\text{H}] \lesssim -0.5$ corresponding to old halo and thick-disk stars, while it tends to show a large scatter

⁵ For example, by using the high-quality Subaru/HDS spectra of BD+44°493 and HD 140283 available to us (visual region, $R \simeq 90000$, S/N ~ 350 and ~ 700 , respectively), we carried out $v_e \sin i$ determinations for these stars, based on the profile fitting for Fe I 5586.77 and Ca I 5588.75 lines following the procedure described in Takeda et al. (2010; cf. section 3 therein). We then obtained almost the same results of $v_e \sin i \simeq 2.3\text{--}2.4 \text{ km s}^{-1}$ for both stars, which suggests that the $v_e \sin i$ values of 3.9 km s^{-1} (BD+44°493) and 5.0 km s^{-1} (HD 140283) given in table 3 of Cortés et al. (2009) are erroneously overestimated.

(many clustering around $\log EW(\text{m}\text{\AA}) \sim 2$ on the average) for comparatively young thin-disk stars at $-0.5 \lesssim [\text{Fe}/\text{H}]$, from which we may speculate that the origin of chromospheres is different between these two star groups.

For the latter group of thin-disk stars, still showing appreciable rotational velocities, stellar rotation may play the decisive role in controlling the chromospheric activity, for which organized magnetic fields generated by rotation-induced dynamo would be responsible, as widely believed. The difference in the rotational velocity would be the reason why *EW*s in this group are diversified.

Meanwhile, the standard rotation/magnetism-induced activity would not be relevant any more for the former group of old halo or thick-disk stars, whose rotational velocity should have been considerably slowed down. Instead, a constant “basal”-level chromospheric activity would come into sight, for which energy dissipation of acoustic waves generated by convection may be a promising heating mechanism. Long-term observations monitoring the activity of old metal-poor stars would be useful to substantiate this hypothesis, since such stars would not show any activity variation.

Yet, we should also keep in mind that this scenario is based on the widely believed hypothesis that stellar rotation generally gets slowed down with age as a result of the magnetic braking effect. It is therefore important to check whether rotational velocities of old metal-poor stars tend to be slower than those of young stars. Given the enormous difficulty of establishing $v_e \sin i$ of considerably slow rotators, however, this would not be an easy task (even the inverse trend is suggested from the literature data of the present sample stars, though its credibility is questionable).

The existence of chromospheres may influence the formation of spectral lines. Since current analysis of stellar spectra such as abundance determinations almost exclusively rely on conventional model atmospheres without any consideration of such a temperature rise, whether and how the difference in the temperature structure of the upper atmosphere makes impact on specific cases may be worth investigation.

We express our heartfelt thanks to Y. Minowa and T.-S. Pyo for their kind advices and helpful support in preparing as well as during the IRCS+AO188 observations.

One of the authors (M. T.-H.) is grateful for a financial support from a grant-in-aid for scientific research (C, No. 22540255) from the Japan Society for the Promotion of Science.

This research has made use of the SIMBAD database operated at CDS, Strasbourg, France, as well as the data obtained from the High Energy Astrophysics Science Archive Research Center (HEASARC), provided by NASA’s Goddard Space Flight Center.

References

Andretta, V., & Giampapa, M. S. 1995, *ApJ*, 439, 405
Asplund, M. 2005, *ARA&A*, 43, 481

Cayrel, R. 1988, in *Proc. IAU Symp. 132, The Impact of Very High S/N Spectroscopy on Stellar Physics*, ed. G. Cayrel de Strobel & M. Spite (Dordrecht: Kluwer), 345
Cayrel de Strobel, G., Soubiran, C., & Ralite, N. 2001, *A&A*, 373, 159
Cortés, C., Silva, J. R. P., Recio-Blanco, A., Catelan, M., Do Nascimento, Jr., J. D., & De Medeiros, J. R. 2009, *ApJ*, 704, 750
Dupree, A. K., Hartmann, L. H., & Smith, G. H. 1990, *ApJ*, 353, 623
Dupree, A. K., Smith, G. H., & Strader, J. 2009, *AJ*, 138, 1485
Hoffleit, D., & Jaschek, C. 1982, *The Bright Star Catalogue*, 4th ed. (New Haven: Yale University Observatory)
Kurucz, R. L., Furenlid, I., Brault, J., & Testerman, L. 1984, *Solar Flux Atlas from 296 to 1300 nm* (Sunspot, New Mexico: National Solar Observatory)
Lambert, D. L. 1987, *ApJS*, 65, 255
Livingston, W., Wallace, L., White, O. R., & Giampapa, M. S. 2007, *ApJ*, 657, 1137
Narain, U., & Ulmschneider, P. 1996, *Space Sc. Rev.*, 75, 453
Noyes, R. W., Hartmann, L. W., Baliunas, S. L., Duncan, D. K., & Vaughan, A. H. 1984, *ApJ*, 279, 763
O’Brien, Jr., G. T., & Lambert, D. L. 1986, *ApJS*, 62, 899
Peterson, R. C., & Schrijver, C. J. 1997, *ApJ*, 480, L47
Peterson, R. C., & Schrijver, C. J. 2001, in *The 11th Cool Stars, Stellar Systems and the Sun*, ASP Conf. Ser. Vol. 223, eds. R. J. García López, R. Rebolo, and M. R. Zapatero (San Francisco: Astronomical Society of the Pacific), 300
Robinson, R. D., Worden, S. P., & Harvey, J. W. 1980, *ApJ*, 236, L155
Rutten, R. G. M., Schrijver, C. J., Lemmens, A. F. P., & Zwaan, C. 1991, *A&A*, 252, 203
Schrijver, C. J. 1987, *A&A*, 172, 111
Schrijver, C. J. 1995, *A&AR*, 6, 181
Smith, G. H., & Churchill, C. W. 1998, *MNRAS*, 297, 388
Smith, G. H., & Dupree, A. K. 1988, *AJ*, 95, 1547
Takeda, Y. 1995, *PASJ*, 47, 463
Takeda, Y., Honda, S., Kawanomoto, S., Ando, H., & Sakurai, T. 2010, *A&A*, 515, A93
Takeda, Y., & Takada-Hidai, M. 2011, *PASJ*, in press (Paper I) (Preprint: arXiv 1009.0824)
Valenti, J. A., & Fischer, D. A. 2005, *ApJS*, 159, 141
Vaughan, Jr., A. H., & Zirin, H. 1968, *ApJ*, 152, 123
Zarro, D. M., & Zirin, H. 1986, *ApJ*, 304, 365
Zirin, H. 1982, *ApJ*, 260, 655

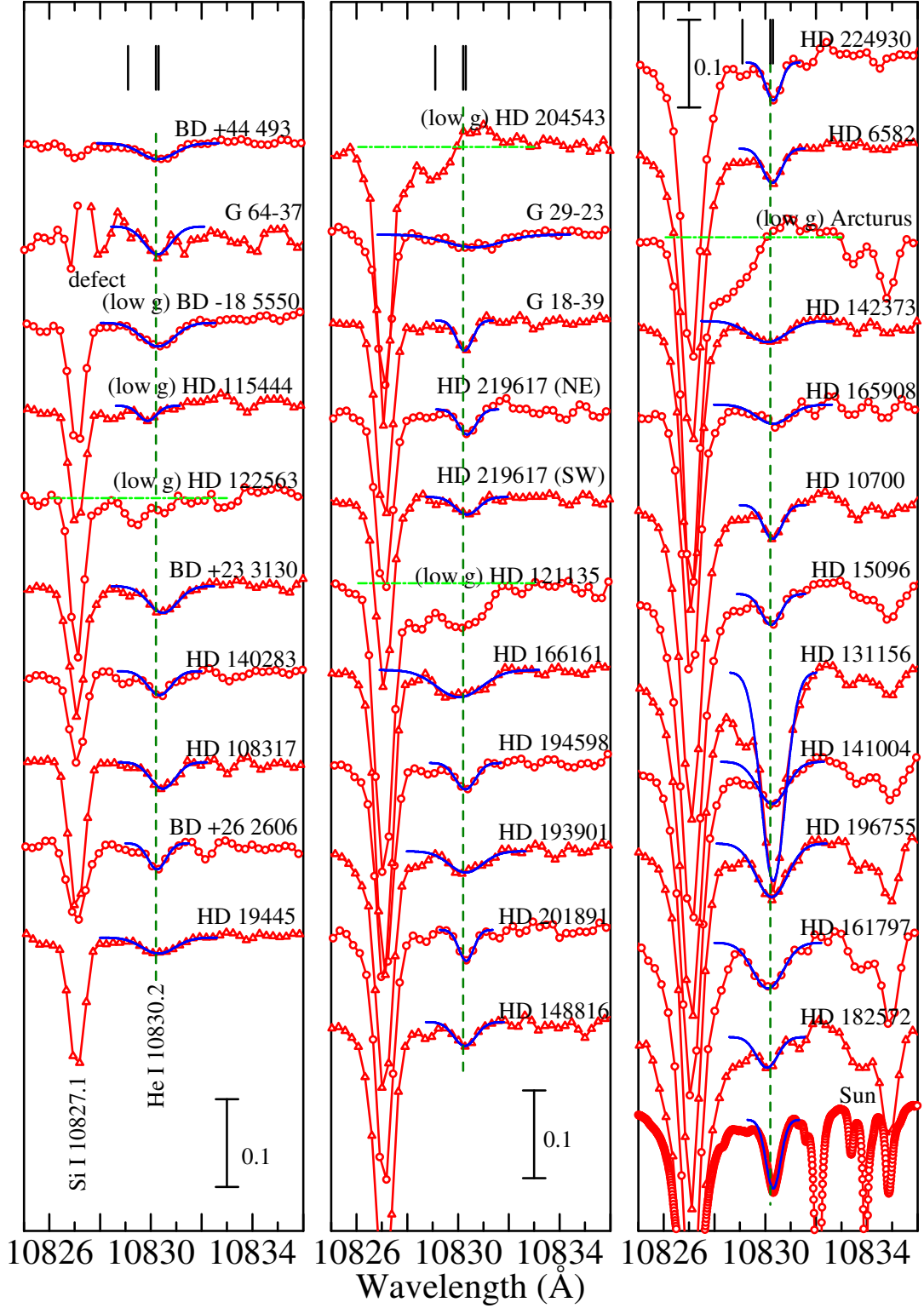


Fig. 2. Observed spectra (red symbols) of 33 target stars (plus the Sun) in the 10825–10836 Å region comprising the Si I 10827 and He I 10830 lines. The Gaussian-fit profiles applied to the He I 10830 line for *EW* measurements are depicted by blue lines. The wavelength positions of three components (10829.088, 10830.247, and 10830.336 Å) are marked by ticks at the top of each panel, while the strength-weighted mean wavelength of 10830.17 Å (almost corresponding to the center of the He I 10830 line) is shown by the vertical dashed line. In each panel (from left to right), the spectra are arranged (from top to bottom) in the ascending order of $[\text{Fe}/\text{H}]$ as in table 1. Each spectrum is shifted by 0.1 relative to the adjacent one. The wavelength scale of each stellar spectrum has been adjusted to the rest frame. Stars indicated with “(low *g*)” at the head of the name are “low-gravity” giants with $1 < \log g < 2$, for which measurements tend to be difficult because they often show complex blue-shifted components (blended with the Si I line) caused by substantial outflow. The Gaussian profiles fitted for *EW* measurements are depicted in blue lines, while only the continuum levels are indicated by green dashed lines for the four “low *g*” cases where measurements could not be done.

Table 1. Program stars and measurement results for the He I 10830 line.

Name	T_{eff} (K)	$\log g$ (cm s^{-2})	v_t (km s^{-1})	[Fe/H] (dex)	V (mag)	f_x/f_{bol} (dex)	R_0	$fwhm$ (Å)	EW (mÅ)	Remark
BD+44°493	5510	3.70	1.30	−3.68	9.13	...	0.018	1.60	31.4	D
G 64-37	6432	4.24	1.50	−3.08	11.14	...	0.032	1.23	41.7	D, insufficient S/N, uncertain
BD−18°5550	4750	1.40	1.80	−3.06	9.35	...	0.027	1.51	43.9	G(lg)
HD 115444	4721	1.74	2.00	−2.71	9.00	...	0.017	0.84	15.5	G(lg), profile not clear, uncertain
HD 122563	4572	1.36	2.90	−2.61	6.20	G(lg), blue shift, abandoned
BD+23°3130	5000	2.20	1.40	−2.60	8.94	...	0.031	1.35	44.3	G
HD 140283	5830	3.67	1.90	−2.55	7.21	...	0.028	1.10	32.5	D
HD 108317	5310	2.77	1.90	−2.35	8.03	...	0.031	1.16	38.0	G
BD+26°2606	5875	4.10	0.40	−2.30	9.73	...	0.030	0.83	26.5	D
HD 19445	6130	4.39	2.10	−2.05	8.05	...	0.018	1.54	30.4	D
HD 204543	4672	1.49	2.00	−1.72	8.60	G(lg), blue shift, abandoned
G 29-23	6194	4.04	1.50	−1.69	10.19	...	0.015	2.53	39.4	D, profile not clear, uncertain
G 18-39	6093	4.19	1.50	−1.46	10.38	...	0.035	0.75	27.9	D
HD 219617(NE)	5825	4.30	1.40	−1.40	*8.16	...	0.029	0.82	25.3	D
HD 219617(SW)	5825	4.30	1.40	−1.40	*8.16	...	0.020	1.08	23.3	D
HD 121135	4934	1.91	1.60	−1.37	9.30	G(lg), blueside blend, abandoned
HD 166161	5350	2.56	2.25	−1.22	8.16	...	0.031	2.10	69.9	G
HD 194598	6020	4.30	1.40	−1.15	8.36	...	0.031	0.94	30.5	D
HD 193901	5699	4.42	1.20	−1.10	8.67	...	0.025	1.55	40.5	D
HD 201891	5900	4.19	1.40	−1.10	7.38	...	0.035	0.69	26.2	D
HD 148816	5860	4.07	1.60	−1.00	7.27	...	0.028	1.03	30.1	D
HD 224930	5275	4.10	1.05	−0.90	5.75	−5.91	0.044	0.70	32.8	D
HD 6582	5331	4.54	0.73	−0.81	5.12	...	0.040	0.86	36.7	D
Arcturus	4281	1.72	1.49	−0.55	−0.04	G(lg), blue shift, abandoned
HD 142373	5776	3.83	1.26	−0.51	4.62	...	0.024	1.74	45.1	D
HD 165908	6183	4.35	1.24	−0.46	5.07	−6.10	0.022	1.56	36.2	D
HD 10700	5420	4.68	0.66	−0.43	3.50	−6.33	0.040	0.87	36.4	D
HD 15096	5375	4.30	0.80	−0.20	7.95	...	0.036	0.90	34.6	D
HD 131156	5527	4.60	1.10	−0.13	4.59	−4.47	0.241	1.13	291.0	D, high-activity star (strong He line)
HD 141004	5877	4.11	1.17	−0.01	4.43	−6.23	0.049	1.35	69.9	D
HD 196755	5750	3.83	1.23	+0.09	5.05	−5.82	0.061	1.45	94.7	D
HD 161797	5580	3.99	1.11	+0.29	3.42	−6.23	0.053	1.41	80.0	D
HD 182572	5566	4.11	1.07	+0.33	5.16	−6.25	0.036	0.99	38.0	D, blueside blend, rather uncertain
Sun	5780	4.44	1.00	0.00	0.080	0.68	58.2	D

In columns 1 through 7 are given the star designation, effective temperature, logarithmic surface gravity, microturbulent velocity dispersion, Fe abundance relative to the Sun, apparent V magnitude, and $\log(f_x/f_{\text{bol}})$ available in the ROSAT data archive (definitely identified cases). See table 1 of Paper I for the source of atmospheric parameters. Columns 8–10 present the results of the measurement for the He I 10830 line: R_0 , $fwhm$, and EW are the line-center depth ($\equiv 1 - f_0/f_{\text{cont}}$), the full-width at half-maximum, and the equivalent width derived from the Gaussian-fit measurement, respectively. The characters in column 10 denote the luminosity/gravity class of each star: “D” is for dwarfs ($\log g > 3$) and “G” is for giants ($\log g < 3$); particularly low-gravity giants ($\log g < 2$) are further marked with “(lg)” (see also footnote 1). Some remarks relevant to specific cases are also given in column 10, when necessary. The objects are arranged in the ascending order of [Fe/H].

* Combined magnitude of the double-star system.